



CHORUS

This is the accepted manuscript made available via CHORUS. The article has been published as:

Highly anisotropic exchange interactions of $j_{\text{eff}}=1/2$
iridium moments on the fcc lattice in
 $\text{La}_{\{2\}}\text{BIrO}_{\{6\}}$ (B=Mg,Zn)

A. A. Aczel, A. M. Cook, T. J. Williams, S. Calder, A. D. Christianson, G.-X. Cao, D. Mandrus,
Yong-Baek Kim, and A. Paramakanti

Phys. Rev. B **93**, 214426 — Published 20 June 2016

DOI: [10.1103/PhysRevB.93.214426](https://doi.org/10.1103/PhysRevB.93.214426)

Highly-anisotropic exchange interactions of $j_{\text{eff}} = 1/2$ iridium moments on the fcc lattice in $\text{La}_2\text{B}\text{IrO}_6$ ($B = \text{Mg}, \text{Zn}$)

A. A. Aczel,^{1,*} A. M. Cook,² T. J. Williams,¹ S. Calder,¹ A.D. Christianson,¹
G.-X. Cao,³ D. Mandrus,^{3,4} Y. B. Kim,^{2,5} and A. Paramekanti^{2,5,†}

¹*Quantum Condensed Matter Division, Oak Ridge National Laboratory, Oak Ridge, TN 37831, USA*

²*Department of Physics, University of Toronto, Toronto, Ontario, Canada M5S 1A7*

³*Materials Science and Technology Division, Oak Ridge National Laboratory, Oak Ridge, TN 37831, USA*

⁴*Department of Materials Science and Engineering, University of Tennessee, Knoxville, TN 37996, USA*

⁵*Canadian Institute for Advanced Research, Toronto, Ontario, M5G 1Z8, Canada*

We have performed inelastic neutron scattering (INS) experiments to investigate the magnetic excitations in the weakly distorted face-centered-cubic (fcc) iridate double perovskites $\text{La}_2\text{ZnIrO}_6$ and $\text{La}_2\text{MgIrO}_6$, which are characterized by A-type antiferromagnetic ground states. The powder inelastic neutron scattering data on these geometrically frustrated $j_{\text{eff}} = 1/2$ Mott insulators provide clear evidence for gapped spin wave excitations with very weak dispersion. The INS results and thermodynamic data on these materials can be reproduced by conventional Heisenberg-Ising models with significant uniaxial Ising anisotropy and sizeable second-neighbor ferromagnetic interactions. Such a uniaxial Ising exchange interaction is symmetry-forbidden on the ideal fcc lattice, so that it can only arise from the weak crystal distortions away from the ideal fcc limit. This may suggest that even weak distortions in $j_{\text{eff}} = 1/2$ Mott insulators might lead to strong exchange anisotropies. More tantalizingly, however, we find an alternative viable explanation of the INS results in terms of spin models with a dominant Kitaev interaction. In contrast to the uniaxial Ising exchange, the highly-directional Kitaev interaction is a type of exchange anisotropy which is symmetry-allowed even on the ideal fcc lattice. The Kitaev model has a magnon gap induced by quantum order-by-disorder, while weak anisotropies of the Kitaev couplings generated by the symmetry-lowering due to lattice distortions can pin the order and enhance the magnon gap. Our findings highlight how even conventional magnetic orders in heavy transition metal oxides may be driven by highly-directional exchange interactions rooted in strong spin-orbit coupling.

PACS numbers: 75.30.Ds, 75.30.Et, 75.47.Lx

I. INTRODUCTION

Magnetic materials with strongly-anisotropic exchange interactions often display exotic magnetic properties and allow fundamental theories of quantum magnetism to be tested in the laboratory¹⁻³. Many interesting studies on these topics have concentrated on systems based on rare earths or 3d transition metals with unquenched orbital angular momentum. For example, the classical spin ice pyrochlores $\text{Dy}_2\text{Ti}_2\text{O}_7$ and $\text{Ho}_2\text{Ti}_2\text{O}_7$ with net ferromagnetic nearest neighbor exchange and dipole interactions are well-described by an Ising Hamiltonian with the moments constrained to lie along the local $\langle 111 \rangle$ directions⁴. Recent studies have shown that such classical spin-ice materials, with ‘two-in, two-out’ magnetic ground states, support emergent monopole excitations⁵, and there is ongoing work aimed at understanding ‘quantum spin-ice’ physics in materials such as $\text{Yb}_2\text{Ti}_2\text{O}_7$ ⁶.

Recently, a novel family of magnetic materials based on strong spin-orbit coupling (SOC) and the d^5 electron configuration, so-called $j_{\text{eff}}=1/2$ Mott insulators, have been attracting great interest⁷, as the relativistic entanglement of the orbital and spin degrees of freedom leads to unusual single ion wavefunctions⁸. Two different types of interactions for these wavefunctions have been considered in the ideal limit of a local cubic environment: superexchange mediated by a single anion via (a) a 90° bond (e.g. edge-sharing octahedra) and (b) a 180° bond (e.g. corner-sharing octahedra).

Superexchange through a 180° bond leads to a Hamiltonian with Heisenberg and anisotropic pseudodipolar terms⁸. Res-

onant inelastic x-ray scattering (RIXS), performed to probe magnons in the single layer iridate Sr_2IrO_4 , shows that its magnetic excitations are consistent with a dominant Heisenberg interaction⁹, with a small gap arising from spin-orbit-induced anisotropic couplings. However, RIXS on the bilayer iridate $\text{Sr}_3\text{Ir}_2\text{O}_7$ provides evidence for a large spin gap ascribed to a significant interplane pseudodipolar term for spins within the bilayer, leading to the spin gap and bandwidth of the magnons having comparable values of 92 and 70 meV respectively¹⁰. Such a pseudodipolar (Ising-like) term is symmetry-allowed in a tetragonal crystal. Its magnitude is thought to be large in $\text{Sr}_3\text{Ir}_2\text{O}_7$ due to the proximity to a metal-insulator transition and a sizable tetragonal distortion of the IrO_6 octahedra, which increase the impact of the Hund’s coupling in the superexchange process as well as promote greater mixing of $j_{\text{eff}} = 1/2$ and $j_{\text{eff}} = 3/2$ states¹⁰.

Superexchange through a 90° bond is even more intriguing. In this geometry, there are two different exchange paths connecting magnetic ions. Projecting the t_{2g} hopping onto the $j_{\text{eff}} = 1/2$ states leads to destructive interference of the hopping amplitudes, suppressing the usual superexchange. Incorporating Hund’s coupling can then lead to a Hamiltonian where anisotropic exchange terms dominate⁸. For the special case of the two-dimensional (2D) honeycomb lattice, the resulting Hamiltonian is called the ‘Kitaev model’¹¹ and it is exactly solvable, with a quantum spin liquid ground state and emergent Majorana fermion excitations.

A true example of a Kitaev spin liquid has, however, remained elusive, as experimental realizations of the 2D honey-

comb lattice such as α -Li₂IrO₃¹², Na₂IrO₃¹³, and α -RuCl₃¹⁴ are characterized by magnetically *ordered* ground states^{15,16} due to non-negligible Heisenberg, off-diagonal, or further neighbor exchange couplings^{17–20}. On the other hand, recent Raman scattering^{21,22} and inelastic neutron scattering (INS)^{23,24} measurements have found evidence for strong Kitaev interactions in α -RuCl₃, suggesting the ordered ground state may be proximate to a quantum phase transition into the Kitaev spin liquid ground state. Finally, recent experiments on the 3D honeycomb polymorphs β/γ -Li₂IrO₃^{25,26} have uncovered complex spiral orders^{27,28}, also ascribed to significant Kitaev exchange^{29,30}.

While the quest to find an experimental example of a Kitaev spin liquid continues, a parallel effort is underway to characterize the magnetic properties of other $j_{\text{eff}}=1/2$ Mott insulators. Systems of particular interest have superexchange mediated by anions through 90° bonds, as they are prime candidates to host Kitaev-type exchange interactions³¹. Exploring cases in which the magnetic ion coordination number is different from the three-fold coordination of the honeycomb motif in previously studied materials should yield further insights into the role of Kitaev interactions in quantum magnetism on other lattices.

Motivated by this background, we study $j_{\text{eff}}=1/2$ Mott insulating double perovskites (DPs) La₂B₂IrO₆ ($B = \text{Mg, Zn}$)^{32–34}, with Ir⁴⁺ ions on the quasi-face-centered cubic (quasi-fcc) lattice. In these materials, the local octahedral environment of the Ir⁴⁺ ions is very close to the cubic limit, and the larger Ir-Ir distance compared with ABO₃ perovskites leads to a Mott insulator, thus suggesting that the $j_{\text{eff}}=1/2$ description is appropriate. Although the DP structure does not feature direct edge-sharing IrO₆ octahedra, it has multiple interfering Ir-O-O-Ir paths. As discussed in detail in the context of the triangular lattice iridate material Ba₃IrTi₂O₉, this can suppress oxygen-mediated hopping of the $j_{\text{eff}}=1/2$ states and lead to significant Kitaev interactions^{35–37}. Since we can simply view the fcc crystal of Ir⁴⁺ ions as a stacking of such triangular lattices along the {111} direction, the analysis in these works also applies to La₂B₂IrO₆. Indeed, the fcc lattice has been theoretically proposed as a potential venue for hosting Kitaev interactions³¹.

The DP fcc structure has new features beyond previous, experimentally-studied, honeycomb-based materials: twelve-fold coordinated Ir sites, strong geometric frustration, and a larger Ir-Ir distance weakening direct Heisenberg exchange. This motivates us to explore the nature of magnetism in these materials in detail. The significance of the Kitaev interactions in La₂B₂IrO₆ is not at all evident from the observed magnetic ordering. Indeed, as explained in detail below, both materials exhibit A-type (Type-I) antiferromagnetic (AFM) ordering, with transition temperatures $T_N = 12$ K for La₂MgIrO₆ and 7.5 K for La₂ZnIrO₆^{33,34,38}. Such commonly observed magnetic order on the fcc lattice can arise purely from a nearest-neighbor Heisenberg AFM exchange interaction. However, we note that in this case the corresponding frustration parameter f , defined as Θ_{CW}/T_N , the ratio of the Curie-Weiss temperature to the AFM ordering temperature, is expected to be large, with $f \approx 9$ for spin-1/2 magnets, whereas the ex-

perimentally determined Curie-Weiss temperatures $\Theta_{CW} \approx -24$ K for La₂MgIrO₆ and $\Theta_{CW} \approx -3$ K for La₂ZnIrO₆ yield small frustration values, $f \approx 2$ and 0.4 respectively³³. One possible way to strongly suppress frustration is to have large ferromagnetic second neighbor coupling^{39,40}. However, as shown in recent theoretical work, even the symmetry-allowed nearest neighbor AFM Kitaev coupling on the fcc lattice cooperates with the nearest neighbor AFM Heisenberg exchange to greatly stabilize A-type AFM. Interestingly, in the regime where this Kitaev interaction dominates, it leads to low f values⁴¹. Given the strong SOC in these materials, this warrants a further exploration of the possible role played by such spin-orbit-induced directional exchange interactions on quantum magnetism in DPs.

The smoking gun signature of any strong anisotropic couplings is most clearly encoded in the quantum spin fluctuations, and it reveals itself in the magnon spectrum. In this paper, we present results from an INS study of the magnetic excitations in La₂B₂IrO₆. Typically, INS is the most powerful technique to probe magnetic excitations in crystals. However, INS generally has severe limitations in most iridates due to an unfavorable magnetic form factor and the strong neutron absorption cross-section of the Ir nuclei, rendering RIXS as the tool of choice to study magnons^{9,10,42}. Remarkably, as shown in Fig. 1, we find that La₂B₂IrO₆ exhibit a clearly observable INS signal, revealing *gapped, highly non-dispersive* magnons. It is likely that the non-dispersive nature of the magnons is what leads to a higher intensity over a small energy window, rendering them clearly visible in the INS measurements unlike for most other iridates. Our INS work is important since RIXS does not yet possess the meV resolution to study low energy magnons in a strong Mott insulator.

A comparison of our INS results with theoretical calculations shows that we can describe the data using conventional Heisenberg-Ising models with a uniaxial Ising exchange anisotropy. However, the uniaxial Ising exchange interaction is symmetry-forbidden on the ideal fcc lattice. This suggests that for such a Heisenberg-Ising model to provide a viable explanation of the data, even weak monoclinic distortions in these $j_{\text{eff}}=1/2$ Mott insulators must, remarkably, be capable of inducing strong exchange anisotropies. We also discuss alternative spin models with dominant Kitaev interactions which are shown to capture the dynamical spin correlations in these materials. In contrast to the uniaxial Ising term, the Kitaev interaction is symmetry-allowed even on the ideal fcc lattice, and weak lattice distortions may induce small anisotropies of the Kitaev coupling. We thus propose that the Kitaev exchange might provide a more natural explanation for the combined INS and thermodynamic observations in these materials. Our study suggests that even the *conventional* A-type AFM order in these geometrically-frustrated magnets may ultimately be selected by highly-anisotropic exchange interactions resulting from the strong spin-orbit coupling of heavy transition metal ions.

This paper is organized as follows: We begin with a discussion of the crystal structure and magnetic ordering patterns for La₂B₂IrO₆ in Sections II and III. We then present the INS data on these materials in Section IV which show evidence for

gapped spin waves. In Section V, we discuss the most likely phenomenological spin wave models needed to describe these results. Section VI discusses the relationship of these models to the experimental data, providing estimates of exchange couplings which can semi-quantitatively reproduce the INS results. Section VII discusses experimental estimates of B/B' site-mixing disorder and its possible qualitative impact on the modelling. Finally, Section VIII concludes with a summary of our work and implications for other materials.

II. II. CRYSTAL STRUCTURE

Ordered double perovskites with the general formula $A_2BB'O_6$ ideally crystallize in a cubic structure, with the B and B' ions occupying two interpenetrating fcc sublattices. $\text{La}_2\text{MgIrO}_6$ and $\text{La}_2\text{ZnIrO}_6$ crystallize in the lower symmetry, monoclinic space group $P2_1/n$, arising from small structural distortions to the cubic structure. The unit cell associated with the $P2_1/n$ space group is a superstructure of the primitive cubic unit cell, which can be approximately indexed in tetragonal notation due to the extremely weak monoclinic distortions. Assuming that \hat{x} , \hat{y} , and \hat{z} are aligned with the three fcc crystallographic directions, the relationships between the tetragonal and fcc lattice constants are as follows: $\vec{a}_t = a_{\text{fcc}}(\hat{x} \pm \hat{y})/2$ and $\vec{c}_t = a_{\text{fcc}}\hat{z}$. For $\text{La}_2\text{BiIrO}_6$, previous x-ray diffraction studies³³ have shown that $a_{\text{fcc}} \approx 7.9 \text{ \AA}$.

We now make an effort here to quantify the magnitudes of the monoclinic structural distortions for the IrO_6 octahedra of $\text{La}_2\text{BiIrO}_6$. The distortions have two main effects: the rotation of the octahedra about both the cubic $[110]$ and c -axes, and the deformation of the Ir^{4+} local environment away from ideal cubic. The rotation angles of the IrO_6 octahedra can be determined according to Ref.⁴³ by using the refined atomic fractional coordinates and the Glazer notation discussed in Refs.^{44,45}. We find that the IrO_6 octahedra have global rotations of 13° and 14° for the Mg and Zn systems respectively about the cubic $[110]$ axis, and rotations of 9° and 11° respectively about the c -axis that are staggered between adjacent ab-layers. The deformation of the IrO_6 octahedra can be quantified by considering the different Ir-O bond lengths and O-Ir-O bond angles. From the structural refinements reported in Ref.³³, we find that the six Ir-O bond lengths are within 1% of each other for both materials, and all O-Ir-O bond angles are within 3.5° (1.5°) of 90° and 180° for the Mg (Zn) system. This implies a nearly-ideal local cubic environment for the Ir^{4+} ions, which is consistent with $j_{\text{eff}}=1/2$ single ion ground states for $\text{La}_2\text{BiIrO}_6$.

III. III. MAGNETIC ORDERING

For $\text{La}_2\text{MgIrO}_6$, magnetization measurements show no evidence for a net ferromagnetic (FM) moment, while neutron powder diffraction work³³ finds a magnetic Bragg peak at $Q = 0.79 \text{ \AA}^{-1}$ corresponding to A-type AFM order. These combined results are consistent with a magnetic propagation vector of $\vec{k} = (0.5 \ 0.5 \ 0)_t$, indicative of FM planes stacked

along the $[110]_t$ direction. Although the data do not determine the moment direction unambiguously, electronic structure calculations³³ predict that the moments lie predominantly in the FM planes (A-II type AFM in the notation of Ref.⁴¹).

For $\text{La}_2\text{ZnIrO}_6$, magnetization measurements find evidence for a net FM moment, while neutron diffraction again detects³³ a magnetic Bragg peak at $Q = 0.79 \text{ \AA}^{-1}$. These findings are consistent with a canted A-type AFM characterized by a $\vec{k} = 0$ propagation vector, which defines the c -axis as the FM plane stacking direction. The magnetic Bragg peak is then uniquely indexed as $(001)_t$. The observation of this peak, combined with the absence of the $(100)_t$ and $(010)_t$ peaks, strongly implies that the ordered moments lie predominantly in the FM planes. Thus, the A-type AFM in this system also corresponds to A-II. The spin canting in $\text{La}_2\text{ZnIrO}_6$ arises from the small, staggered IrO_6 octahedral rotations ($\sim 11^\circ$).

IV. IV. INELASTIC NEUTRON SCATTERING RESULTS

We next present our new results on the magnetic excitations associated with the ordered phases of these materials. Inelastic neutron scattering data were collected on previously synthesized³³ powder samples of $\text{La}_2\text{BiIrO}_6$ at the HYSPEC spectrometer of the Spallation Neutron Source, Oak Ridge National Lab (ORNL). The powder samples were loaded in Al annular cans to minimize neutron absorption. All data were collected using incident energies of $E_i = 7.5$ and 15 meV, with corresponding Fermi chopper frequencies of 240 and 300 Hz, resulting in instrumental energy resolutions of 0.3 and 0.7 meV (Gaussian full-width half-maximum [FWHM]) respectively at the elastic line. A He cryostat was used to achieve a base temperature of 1.5 K. Empty Al annular can measurements were subtracted from all the HYSPEC data presented in this work, so the Al scattering contribution to the sample spectra would be minimized. INS data for these systems were also collected using a He cryostat on the thermal triple axis spectrometer HB-3 at the High Flux Isotope Reactor of ORNL. A collimation of $48^\circ\text{-}60^\circ\text{-}60^\circ\text{-}120^\circ$ and a fixed final energy of $E_f = 14.7$ meV were used to achieve an energy resolution of 1.2 meV at the elastic line (Gaussian FWHM).

Fig. 1(a) and (b) depict color contour plots of the coarser energy resolution $E_i = 15$ meV HYSPEC data at $T = 1.5$ K, where a nearly-dispersionless excitation band is visible for both materials. Note that the lowest- Q regions in these plots show no intensity; this issue results from a background over-subtraction of the direct beam, which is a consequence of the strong neutron absorption of Ir in the samples. The observed excitations are clearly magnetic in origin, as they decrease in intensity with increasing Q . They are also no longer visible above T_N , with only quasi-elastic scattering remaining, as shown in panels (c) and (d). Color contour plots of the finer energy resolution $E_i = 7.5$ meV HYSPEC data are presented in Fig. 1(e) and (f). The same excitations are still present in the data, which indicates that they are not spurious in nature. Fig. 1(g) and (h) show constant- $\hbar\omega$ cuts through the fine-resolution data for the two materials, with an integration range of $[0.6, 1]$ meV. We find no evidence for enhanced in-

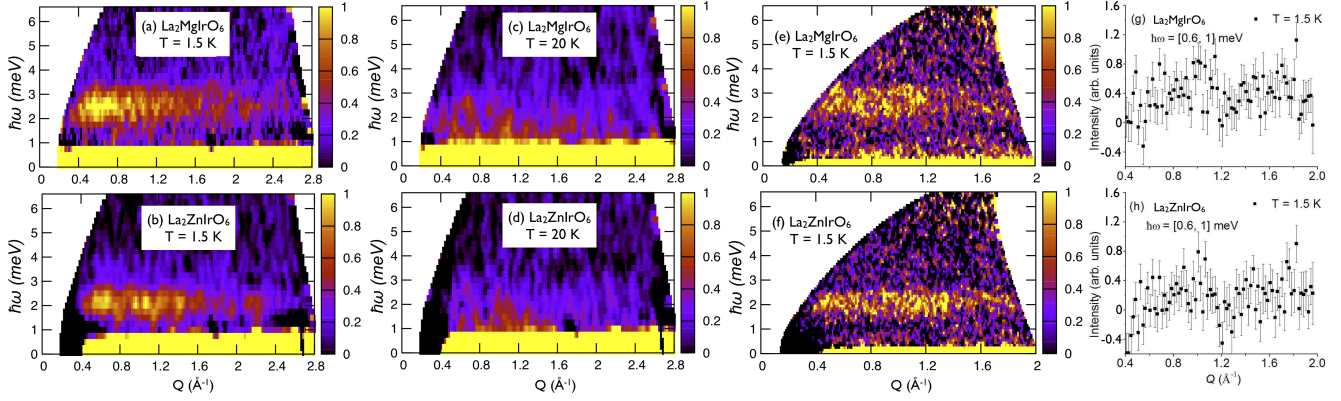


FIG. 1: (Color online) Color contour plots of the coarse energy resolution HYSPEC data for (a) $\text{La}_2\text{MgIrO}_6$ and (b) $\text{La}_2\text{ZnIrO}_6$ with $E_i = 15$ meV and $T = 1.5$ K. Inelastic modes with weak dispersion are clearly observed for both materials. The color contour plots with $E_i = 15$ meV and $T = 20$ K shown in panels (c) and (d) indicate that these modes disappear above the respective T_N 's of 12 K and 7.5 K for the Mg and Zn systems, which suggests that they have a magnetic origin. Panels (e) and (f) depict similar color contour plots for $\text{La}_2\text{MgIrO}_6$ and $\text{La}_2\text{ZnIrO}_6$ at $T = 1.5$ K, but with better energy resolution arising from the choice of $E_i = 7.5$ meV. The same excitations are visible in these inelastic spectra. Note that the lowest- Q regions in the color contour plots show no intensity; this issue results from a background oversubtraction of the direct beam, which is a consequence of the strong neutron absorption of Ir in the samples. Panels (g) and (h) show constant- $\hbar\omega$ cuts through the $T = 1.5$ K fine-resolution datasets with an integration range of $[0.6, 1]$ meV. The lack of increased intensity near the magnetic zone center $Q = 0.79 \text{ \AA}^{-1}$ for each system indicates that the magnetic excitations are fully-gapped.

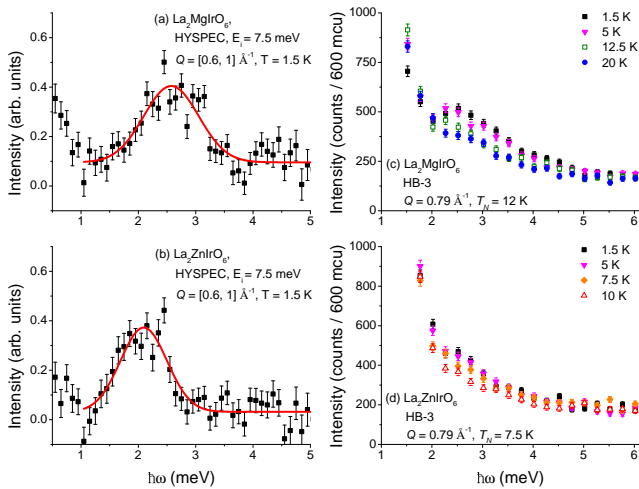


FIG. 2: (Color online) (a), (b) Constant- Q cuts through the HYSPEC data shown in Fig. 1(e) and (f), integrated over $Q = [0.6, 1] \text{ \AA}^{-1}$. These cuts clearly show that the inelastic modes are gapped in each case. Gaussian fits are superimposed on the data, which were used to determine the peak positions. For $\text{La}_2\text{MgIrO}_6$, the mode is centered at $\hbar\omega = 2.57(4)$ meV, and for $\text{La}_2\text{ZnIrO}_6$, it is centered at $2.09(3)$ meV. (c), (d) HB-3 constant- Q scans with $Q = 0.79 \text{ \AA}^{-1}$ for $\text{La}_2\text{MgIrO}_6$ and $\text{La}_2\text{ZnIrO}_6$ at selected temperatures. The spin gaps close around T_N for each compound, indicating that the modes have a spin wave origin. Note that 1 mcu (monitor count unit) ≈ 10000 and 11000 monitor counts for the Mg and Zn data respectively.

tensity near the $Q = 0.79 \text{ \AA}^{-1}$ magnetic Bragg peaks, which suggests that these excitations are fully-gapped. Finally, as shown in Fig. 2(a) and (b), a low- T constant- Q cut through

the fine-resolution data centered about the magnetic zone center $Q = 0.79 \text{ \AA}^{-1}$ reveals that the central position of the mode is $2.57(4)$ meV for $\text{La}_2\text{MgIrO}_6$ and $2.09(3)$ meV for $\text{La}_2\text{ZnIrO}_6$, with a FWHM in each case of ~ 1 meV.

We have also carried out detailed temperature-dependent measurements on the thermal triple axis spectrometer HB-3. Fig. 2(c) and (d) present constant- Q scans at a magnetic zone center ($Q = 0.79 \text{ \AA}^{-1}$) for $\text{La}_2\text{MgIrO}_6$ and $\text{La}_2\text{ZnIrO}_6$ respectively. The two panels provide strong evidence that the spin gaps close around T_N in each case, with spectral weight shifting down to lower energies with increasing T . This observed temperature-dependence of the modes indicates that they likely correspond to spin waves. In fact, a crystal field interpretation can be ruled out by considering the typical single ion energy level scheme for $j_{\text{eff}} = 1/2$ Mott insulators. For this class of materials, the lowest-lying excited state to the $j_{\text{eff}} = 3/2$ band is separated from the $j_{\text{eff}} = 1/2$ ground state by $3\lambda_{SO}/2$, where λ_{SO} is the spin-orbit coupling constant. The typical energy scale for this crystal field excitation is on the order of 100's of meV due to large λ_{SO} ^{24,46,47}, which is certainly incompatible with the energy scale of the magnetic modes observed here. With the magnetic excitations for $\text{La}_2\text{BiIrO}_6$ now unambiguously identified as spin waves, we turn to a theoretical modeling of these results.

V. V. THEORY

The observed spin gap and weakly-dispersive spectra in the INS measurements, with the gap being comparable to or even larger than the magnon bandwidth, are suggestive of a nearly Ising-like exchange. Below, we examine the possible origins of this large exchange anisotropy in $\text{La}_2\text{BiIrO}_6$.

The strategy we follow to construct the spin model is very similar to that for other perovskite iridates⁸: namely, we start by assuming an ideal lattice (fcc), with no rotations or tilts of the IrO_6 octahedra, and consider all possible symmetry-allowed exchange couplings. In this ideal fcc limit, the uniaxial Ising exchange interaction, which is the simplest anisotropic exchange interaction typically used to model such gapped magnon spectra, is *symmetry-forbidden*. However, even in this ideal limit, the highly-directional Kitaev interaction and an off-diagonal symmetric exchange are allowed by symmetry⁴¹.

Moving away from the ideal fcc limit, the weak monoclinic distortions, arising from the rotations and tilts of the IrO_6 octahedra, permit a large variety of new exchange terms just on symmetry grounds. A set of such exchange couplings induced by non-cubic distortions have been discussed in previous work in the context of double perovskites^{48,49}. However, given the large number of new terms and the limited data, we choose to focus on the simplest case of a tetragonal crystal distortion⁴⁹ which allows for only a subset of all the terms; in particular, we focus on two new anisotropies which are symmetry-allowed under such a distortion. First, the tetragonal distortion allows for the Kitaev interaction to be different in one crystal plane compared with the other two orthogonal planes. Second, the tetragonal distortion picks a unique axis, thus now permitting a uniaxial Ising interaction.

Below, we study the spin wave dispersion in such spin models and show that they can provide a reasonable description of the INS data. For ease of presentation, we begin by first discussing the conventional and simpler Heisenberg-Ising models with uniaxial Ising exchange, which might apply to non-ideal fcc lattices, followed by a study of the Kitaev-dominant models which begin from the ideal fcc limit. We then argue that the Kitaev-dominant models appear to provide a more reasonable explanation of the combined INS data and previous measurements of Θ_{CW} and T_N .

A. A. Heisenberg-Ising models with uniaxial Ising exchange

Let us begin with the conventional and phenomenological viewpoint that the spin gaps in many of these DPs simply arise from uniaxial Ising interactions. We emphasize that such uniaxial Ising couplings are *symmetry-forbidden* on the ideal fcc lattice; however, they may be permitted in the presence of distortions away from the ideal fcc limit. Limiting ourselves to short-range exchange, such a Heisenberg-Ising Hamiltonian, where different spin components interact with different strengths, is given by

$$H_{HI} = \sum_{\langle \mathbf{r}\mathbf{r}' \rangle} J_1^\mu S_{\mathbf{r}}^\mu S_{\mathbf{r}'}^\mu + \sum_{\langle\langle \mathbf{r}\mathbf{r}' \rangle\rangle} J_2^\mu S_{\mathbf{r}}^\mu S_{\mathbf{r}'}^\mu \quad (1)$$

where $\langle \cdot \rangle$ and $\langle\langle \cdot \rangle\rangle$ refer to nearest and next-nearest neighbor sites. We set $J_{1,2}^y = J_{1,2}^z = J_{1,2}$ and $J_{1,2}^x = (1 + \lambda_{1,2})J_{1,2}$. For $J_2 > 0$, we select $\lambda_1 > 0$ and $\lambda_2 < 0$ which have been shown⁵⁰ to stabilize A-II type AFM when the anisotropy is strong enough to overcome the AFM J_2 . For $J_2 < 0$, we fix $\lambda_{1,2} > 0$.

The powder-averaged dynamic structure factors $S(Q, \omega)$ for these models are shown in Fig. 3 for various values of J_2/J_1 and anisotropies λ_1, λ_2 . It is clear from Fig. 3 that $S(Q, \omega)$ exhibits a high intensity band of gapped dispersionless excitations which resembles the INS data, for either sign of J_2 and varying degrees of anisotropy. We also show the corresponding frustration parameters f_H . We obtain them from the powder averaged $\theta_{CW} = -J_1(3 + \lambda_1) - J_2(3 + \lambda_2)/2$, with T_N determined from classical Monte Carlo simulations rescaled by $S(S + 1)$ to account for quantum effects. We note that for models with AFM $J_2 \geq 0$, the frustration parameter f_H is large even for significant anisotropy $\lambda_{1,2} \sim \mathcal{O}(1)$, approaching the experimentally relevant regime of small frustration $f_H \sim 2$ only for extremely strong uniaxial anisotropy. However, is it reasonable to assume such an extreme uniaxial Ising anisotropy $\lambda_{1,2} > \mathcal{O}(1)$?

To answer this question, we begin by noting that models with large uniaxial Ising exchange anisotropy adequately describe qualitatively-similar INS spectra in certain $3d$ -transition metal ion based magnets such as CsCoCl_3 and CsCoBr_3 ^{51,52}. In these two Co^{2+} systems, the comparable values for SOC (~ 28 meV for CsCoCl_3 ⁵³) and the non-cubic crystal field distortion parameter δ in the single ion Hamiltonian lead to the large uniaxial Ising anisotropies ($\lambda \approx 7 - 8$ ⁵¹). In $\text{La}_2\text{BiIrO}_6$, a similarly large uniaxial Ising anisotropy with a single ion origin should be accompanied by a complete breakdown of the $j_{\text{eff}}=1/2$ description, with a significant modification of the isotropic single ion ground state wavefunctions⁴⁶. However, this breakdown is unlikely, as the SOC scale is expected to be on the order of 100's of meV and much larger than δ . Indeed, the Ir^{4+} local octahedral environments in $\text{La}_2\text{BiIrO}_6$ are amongst the closest to ideal cubic of any $j_{\text{eff}}=1/2$ Mott insulating candidates⁴⁶. Furthermore, recent RIXS measurements have validated a $j_{\text{eff}}=1/2$ ground state for Na_2IrO_3 ⁴⁷, which exhibits much larger IrO_6 octahedral distortions.

Among other iridates, RIXS work on the stacked bilayer material $\text{Sr}_3\text{Ir}_2\text{O}_7$, has shown that the spin waves exhibit a significant magnon gap¹⁰. This has been understood as a result of a significant uniaxial Ising exchange ($\lambda \sim 1.4$) between spins on adjacent planes in the bilayer which is comparable to the Heisenberg exchange. The large magnitude of this term in $\text{Sr}_3\text{Ir}_2\text{O}_7$ arises from the sizable tetragonal distortions of the IrO_6 octahedra, and the proximity to a metal-insulator transition; this leads to increased mixing of $j_{\text{eff}}=1/2$ and $j_{\text{eff}}=3/2$ states and a greater impact of Hund's coupling on intermediate states in the superexchange process⁹. Neither of these effects, the strong tetragonal distortions or proximity to a metal-insulator transition, are applicable for $\text{La}_2\text{BiIrO}_6$ since they are in the Mott insulating regime³³ and have nearly cubic IrO_6 octahedra.

A more complete theory^{49,54} for the magnetic excitations of $\text{La}_2\text{BiIrO}_6$ must incorporate antisymmetric Dzyaloshinskii-Moriya (DM) interactions arising from octahedral rotations. However, previous work on Sr_2IrO_4 shows that the effect of octahedral rotations in these $j_{\text{eff}}=1/2$ Mott insulators may be largely accounted for by making local spin rotations on the Heisenberg model⁸, so the Ir moments track the lo-

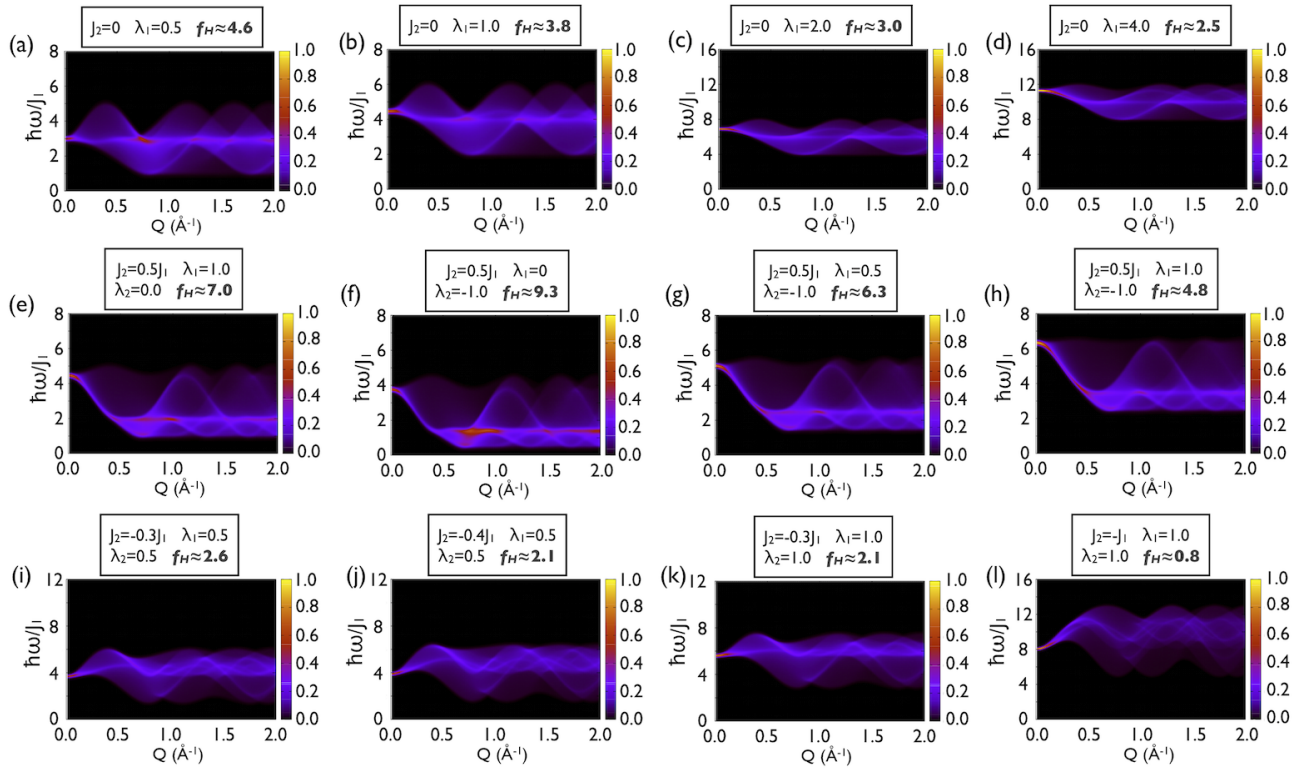


FIG. 3: (Color online) Theoretical powder-averaged $S(Q, \omega)$ for the Heisenberg-Ising models around the A-II AFM ground state considered in the text within linear spin-wave theory with nearest neighbor AFM Heisenberg $J_1 = 1$, various second neighbor Heisenberg exchange J_2 , and varying degrees of uniaxial anisotropies $\lambda_{1,2}$ in the first and second neighbor exchanges. We set $J_{1,2}^y = J_{1,2}^z = J_{1,2}$ and $J_{1,2}^x = (1 + \lambda_{1,2})J_{1,2}$. (a-d) Models with only first neighbor exchange, with $J_2 = 0$. The corresponding frustration parameters f_H are also shown, and range from $f_H \approx 9$ for the isotropic case with $\lambda_1 = 0$ to $f_H \approx 2$ for extreme anisotropy $\lambda_1 \gg 1$. (e-h) Heisenberg-Ising models with AFM second neighbor exchange, $J_2 > 0$, and varying degrees of anisotropy. (i-l) Heisenberg-Ising models with FM second neighbor exchange, $J_2 < 0$, and varying degrees of anisotropy. We have incorporated a small energy broadening in all panels to account for the finite instrumental energy resolution of HYSPEC.

cal octahedral rotations⁵⁵. This ‘rotated’ Hamiltonian features DM interaction and additional terms, which however does not change the spectrum since it is related by a unitary transformation to the Heisenberg model. This hidden Heisenberg symmetry^{8,56} explains the existence of highly dispersive and nearly-gapless magnetic excitations in Sr_2IrO_4 ^{9,57,58}. In bilayer $\text{Sr}_3\text{Ir}_2\text{O}_7$, which has staggered IrO_6 octahedral rotations about the c -axis of $\sim 12^\circ$ ⁵⁹ and a large magnon gap, it is important to note that the pseudodipolar interaction which is thought to be responsible for the gap would be symmetry-allowed even in the *absence* of octahedral rotations, and therefore this term does not arise solely from these rotations⁹. Thus, although $\text{La}_2\text{BiIrO}_6$ with their $P2_1/n$ structure have comparable IrO_6 octahedral rotations to $\text{Sr}_3\text{Ir}_2\text{O}_7$ (albeit about two different crystallographic axes), these rotations alone cannot be responsible for any large new exchange couplings which do not arise from already symmetry-allowed exchange couplings in the ideal fcc lattice.

The above arguments suggest that the regime of extreme and dominant uniaxial Ising anisotropy, $\lambda_{1,2} > \mathcal{O}(1)$, is unlikely for $\text{La}_2\text{BiIrO}_6$, so this subset of models is no longer considered here. We also note that the Heisenberg-Ising models with $J_2 > 0$ and $\lambda_{1,2} \sim \mathcal{O}(1)$ yield frustration param-

eters, $f_H \sim 5-9$ (see Fig. 3), significantly larger than the measured values $f \sim 0.4-2$ ³³, and therefore these models are unlikely to explain the data on $\text{La}_2\text{BiIrO}_6$ either. On the other hand, we find that choosing FM $J_2 < 0$ does lead to models with smaller frustration parameters. In this case, as shown in Fig. 3, we find that we can explain the magnon gap as well as the frustration parameter, but only by choosing significant anisotropies $\lambda_{1,2} \sim \mathcal{O}(1)$.

Our main observation here is that within this class of phenomenological Heisenberg-Ising models, we can only explain the combined INS and thermodynamic data by invoking significant uniaxial Ising anisotropy, as well as significant FM second neighbor exchange. We next explore competing models with dominant Kitaev interactions which provide an unconventional exchange anisotropy, which is symmetry-allowed even in the ideal fcc limit.

B. Models with dominant Kitaev exchange

We have previously studied the classical phase diagram for ideal $j_{\text{eff}} = 1/2$ fcc magnets⁴¹, keeping all symmetry-allowed nearest neighbor (NN) interactions including Heisenberg, Ki-

taev, and off-diagonal symmetric exchange^{19,41,60}. A key finding, relevant to La_2BIrO_6 , was that while the simple NN AFM Heisenberg model exhibits A-type AFM order, this exact same order is also favored in the regime of dominant AFM Kitaev exchange. By contrast, while a small off-diagonal symmetric exchange does not significantly affect our results, a dominant value of this coupling leads to ordered moments pointing along the $\langle 111 \rangle$ direction⁴¹ which does not agree with previous neutron diffraction work for La_2BIrO_6 ³³. One might distinguish between the regimes of weak and dominant Kitaev interactions by using the frustration parameter, f . For the NN Heisenberg AFM model on the fcc lattice, we estimated $f \approx 9$ for spin-1/2 moments⁴¹. However, these iridates exhibit robust AFM order, with experimental values for $f \lesssim 2$, suggesting that SOC-induced Kitaev interactions are large, suppressing frustration and enhancing T_N . This led us to propose a Heisenberg-Kitaev model on the ideal fcc lattice,

$$H = J_1 \sum_{\langle \mathbf{r}\mathbf{r}' \rangle} \vec{S}_{\mathbf{r}} \cdot \vec{S}_{\mathbf{r}'} + J_2 \sum_{\langle\langle \mathbf{r}\mathbf{r}' \rangle\rangle} \vec{S}_{\mathbf{r}} \cdot \vec{S}_{\mathbf{r}'} + H_K \quad (2)$$

$$H_K = J_K \sum_{\langle \mathbf{r}\mathbf{r}' \rangle_{yz}} S_{\mathbf{r}}^x S_{\mathbf{r}'}^x + J_K \sum_{\langle \mathbf{r}\mathbf{r}' \rangle_{xz}} S_{\mathbf{r}}^y S_{\mathbf{r}'}^y + J_K \sum_{\langle \mathbf{r}\mathbf{r}' \rangle_{xy}} S_{\mathbf{r}}^z S_{\mathbf{r}'}^z \quad (3)$$

with $J_K \gg J_1, J_2$, as a better starting point to describe the magnetism in La_2BIrO_6 . Here, $\langle \mathbf{r}\mathbf{r}' \rangle$ and $\langle\langle \mathbf{r}\mathbf{r}' \rangle\rangle$ denote first and second neighbors on the fcc lattice, while $\langle \mathbf{r}\mathbf{r}' \rangle_{yz}$ denotes nearest neighbors in the yz -plane (similarly for xz, xy). This model has a powder averaged $\Theta_{CW} = -J_K - 3J_1 - 3J_2/2$, so if the Kitaev coupling is dominant then $J_K > 0$ is consistent with the reported $\Theta_{CW} < 0$ for La_2BIrO_6 ³³. A classical Monte Carlo study⁴¹ of this model for $J_2 = 0$ and $J_K/J_1 \gg 1$ showed that $f \approx 2$, in reasonable agreement with the data on $\text{La}_2\text{MgIrO}_6$. Here, we focus on the effects of quantum spin fluctuations and the resulting dynamic structure factor of such Kitaev-dominant models.

The AFM Heisenberg-Kitaev model on the fcc lattice leads to A-type AFM, with spins in the FM plane (A-II AFM) for $J_K > 0$, consistent with the discussed magnetic order of La_2BIrO_6 . This order persists in the regime $J_K/J_1 \rightarrow \infty$, so we focus here on the pure Kitaev interaction (i.e., setting $J_1 = J_2 = 0$), in order to study the effect of quantum fluctuations around the A-II state⁶¹. Considering FM xy -planes stacked antiferromagnetically along \hat{z} , and spins making an angle ϕ with the \hat{x} -axis (Ir-O bond direction), linear spin-wave theory leads to the dispersion

$$\omega_{\phi}(\mathbf{k}) = 2J_K [(1 + C_{\mathbf{k}}^{xy})(1 + C_{\mathbf{k}}^{xz} \cos^2 \phi + C_{\mathbf{k}}^{yz} \sin^2 \phi)]^{1/2} \quad (4)$$

with $C_{\mathbf{k}}^{ij} = \cos k_i \cos k_j$ ($i = x, y, z$). The zero-point energy of quantum fluctuations is $E_{zp}(\phi) = \frac{1}{2} \int_{\mathbf{k}} \omega_{\phi}(\mathbf{k})$ per spin exhibits discrete minima at $\phi = n\pi/2$ ($n = 0, 1, 2, 3$). Quantum fluctuations in the presence of SOC thus break the accidental degeneracy in ϕ of the classical Kitaev model, favoring spins to point along the Ir-O bond directions in the FM plane. The magnon dispersion $\omega_{\phi}(\mathbf{k})$ in linear spin wave theory is gapless due to this classical degeneracy.

Since quantum fluctuations lift the classical XY degeneracy of the Kitaev model, we expect the concomitant development

of a magnon gap in the A-II state; indeed, magnon interaction effects, discussed below, gap out this ‘pseudo-Goldstone’ mode. Such an order-by-disorder gap has been discussed within different models for LaTiO_3 ⁶² and the rare-earth pyrochlore $\text{Er}_2\text{Ti}_2\text{O}_7$ ⁶³. In LaTiO_3 , the SOC is weak, leading to a tiny gap for highly-dispersive magnons. In $\text{Er}_2\text{Ti}_2\text{O}_7$, the order-by-disorder gap was recently determined in INS to be ≈ 0.053 meV⁶⁴, about an order of magnitude smaller than the observed energy scale (~ 0.5 meV) of its zone boundary magnetic excitations^{63,64}.

To see the emergence of this spin gap in our Kitaev model in a transparent manner, we expand the above expression for the zero point energy, $E_{zp}(\phi) \approx E_{zp}(\phi = 0) + \frac{1}{2}\gamma\phi^2$, where:

$$\gamma = J_K \int_{\mathbf{k}} \sqrt{\frac{1 + C_{\mathbf{k}}^{xy}}{1 + C_{\mathbf{k}}^{xz}}} (C_{\mathbf{k}}^{yz} - C_{\mathbf{k}}^{xz}). \quad (5)$$

This leads to a pinning field 2γ in the ordered state, which is responsible for gapped magnons. This magnon gap appears naturally within higher order spin-wave theory - incorporating magnon interactions using a self-consistent mean field theory (see Appendix) yields a magnon gap $\approx 0.4J_K$.

Using this mean field approach, we have also computed the renormalized staggered magnetization, and find $m_{AF} \approx 0.46$ in the ideal fcc lattice Kitaev model, leading to $\sim 8\%$ suppression of the classical $j_{\text{eff}} = 1/2$ order parameter due to quantum fluctuations. Taking into account the staggered octahedral rotation $\approx 11^\circ$ in $\text{La}_2\text{ZnIrO}_6$ this $0.92\mu_B$ staggered magnetization translates into a uniform magnetization $\approx 0.18\mu_B$, which roughly agrees with the measured value $\approx 0.22\mu_B$ in $\text{La}_2\text{ZnIrO}_6$ ³³. We have previously argued⁴¹ that the absence of a uniform magnetization in $\text{La}_2\text{MgIrO}_6$ might stem from the axes of staggered octahedral rotations and the stacking direction of FM planes of the A-type AFM order being perpendicular to each other (see Fig. 5 of Ref.⁴¹); this remains to be verified in future experiments.

Using this mean field approach, we have computed the powder averaged dynamic structure factor $S(Q, \omega)$, which is plotted in Fig. 4(f). Our results show that the order-by-disorder gap is about a factor of 5 smaller than the typical energy scale of zone boundary magnon excitations. This relative scale for the gap appears to be in line with the results found using different methods for $\text{Er}_2\text{Ti}_2\text{O}_7$ ⁶³, given the four-fold XY anisotropy for La_2BIrO_6 as opposed to the six-fold anisotropy in $\text{Er}_2\text{Ti}_2\text{O}_7$.

Since La_2BIrO_6 exhibit weak monoclinic distortions, magnon gaps may also be generated from inequivalent Kitaev couplings in different planes (yz, zx, xy). To understand the impact of such anisotropic Kitaev couplings, we have studied a set of Kitaev models with

$$H_K = J_K^x \sum_{\langle \mathbf{r}\mathbf{r}' \rangle_{yz}} S_{\mathbf{r}}^x S_{\mathbf{r}'}^x + J_K \sum_{\langle \mathbf{r}\mathbf{r}' \rangle_{xz}} S_{\mathbf{r}}^y S_{\mathbf{r}'}^y + J_K \sum_{\langle \mathbf{r}\mathbf{r}' \rangle_{xy}} S_{\mathbf{r}}^z S_{\mathbf{r}'}^z \quad (6)$$

where $J_K^x = J_K(1 + \lambda_K)$. Choosing $\lambda_K > 0$ then leads to moments ordered along S_x . In this case, a spin gap is already present in linear spin wave theory; incorporating magnon interactions leads to a slight enhancement of the spin gap.

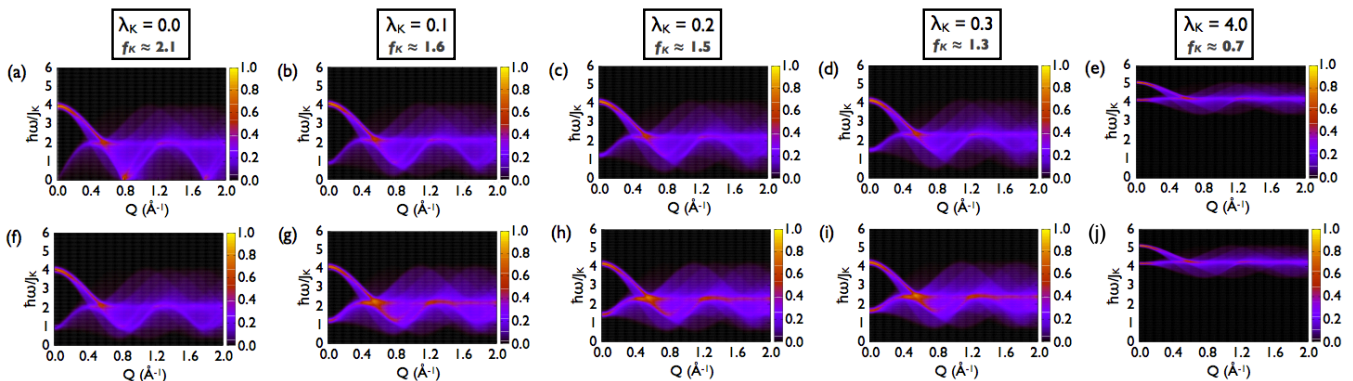


FIG. 4: (Color online) Theoretical powder-averaged $S(Q, \omega)$ for the Kitaev models around the A-II AFM state for indicated spatial anisotropy λ_K . (a-e) Kitaev model within linear spin wave theory for the ideal fcc limit ($\lambda_K = 0$, no spin gap) and various anisotropies ($\lambda_K \leq 4$). (f-j) Kitaev models incorporating magnon interactions which induce an order-by-disorder spin gap even for $\lambda_K = 0$, and a slight enhancement of the spin gap for $\lambda_K > 0$. The corresponding frustration parameters f_K are also shown, they range from $f_K \approx 2$ for the ideal fcc lattice to smaller values with increasing λ_K . We have incorporated a small energy broadening in all panels to account for the finite instrumental energy resolution of HYSPEC.

We plot the corresponding powder-averaged dynamic structure factors in Fig. 4 for various values of λ_K . We have also computed the frustration parameter f_K for this series of Heisenberg-Kitaev models in the regime where $J_K \gg J_1, J_2$, using the powder-averaged value of the Curie-Weiss temperature $\theta_{CW} = -J_K(1 + \lambda_K/3) - 3J_1 - 3J_2/2$, and T_N obtained from classical Monte Carlo simulations with scaling by $S(S+1)$ to account for quantum effects for $S=1/2$. As shown in Fig. 4, f_K is in the range of experimental values $f \lesssim 2$.

VI. VI. COMPARISON WITH EXPERIMENTAL DATA

We next turn to a comparison between the theoretical models and the INS and thermodynamic data in order to obtain some estimates of exchange parameters. For the $S(Q, \omega)$ plots, we use the kinematic cutoff arising from an incident neutron energy $E_i = 7.5$ meV, which is applicable to the particular dataset that we are modeling, and include the Ir^{4+} form factor, which leads to a decay of intensity with increasing Q .

Heisenberg-Ising model: We find that for $\text{La}_2\text{MgIrO}_6$, choosing $J_1 = 0.5$ meV, a second neighbor FM Heisenberg coupling $J_2 = -0.3J_1$, and uniaxial anisotropies $\lambda_1 = \lambda_2 = 1$, leads to a reasonable description of the INS data as shown in Fig. 5(a). For this choice of parameters, we obtain $\Theta_{CW} \approx -24\text{K}$ and $T_N \approx 11\text{K}$, in good agreement with the thermodynamic data. For $\text{La}_2\text{ZnIrO}_6$, since it has a much smaller frustration parameter, we find that we have to incorporate much larger ferromagnetic J_2 . Choosing $J_1 = 0.2$ meV, $J_2 = -J_1$, and $\lambda_1 = \lambda_2 = 1$, leads to $S(Q, \omega)$ shown in Fig. 5(b). With these parameters, we obtain $\Theta_{CW} \approx -7\text{K}$ and $T_N \approx 9\text{K}$, again in good agreement with thermodynamic measurements.

Kitaev-dominant model: For $\text{La}_2\text{MgIrO}_6$, choosing $J_K = 1.7$ meV, a weak anisotropy $\lambda_K = 0.2$, and a small AFM second-neighbor Heisenberg coupling $J_2 = 0.2J_K$, leads to reasonable agreement with the INS data as seen from Fig. 5(c). Using these parameters, we find $\Theta_{CW} \approx -27\text{K}$

and $T_N \approx 14\text{K}$; both these results are in good agreement with the experimental data. We find that incorporating a nonzero J_1 worsens the agreement with the data; this may possibly suggest that J_1 gets suppressed due to the interfering Ir-O-O-Ir pathways. For $\text{La}_2\text{ZnIrO}_6$, we suggest that a weak ferromagnetic second neighbor exchange might be a plausible route to the smaller frustration parameter. As shown in Fig. 5(d), we can get a reasonable description of the magnon dispersion with $J_K \approx 0.7\text{meV}$, $\lambda_K = 0.2$, and $J_2 = -0.2J_K$. In this case, we find $T_N = 8\text{K}$ and $\Theta_{CW} = -6\text{K}$, again in good agreement with experiments.

Interestingly, the sign change of J_2 between the two materials in such Kitaev-dominant models seems to correlate with expectations for DPs with magnetic 3d transition metals on the B' site only. In these materials with lighter magnetic ions, SOC is negligible, so the Hamiltonian is generally assumed to consist of J_1 and J_2 Heisenberg terms only. The choice of magnetic ground state then arises from the signs and relative magnitudes of these two terms, as established previously by mean field theory⁴⁰. Based on the known magnetic ground states of several materials in this family⁶⁵⁻⁷⁴, we have made the empirical observation that a d^0 configuration for the non-magnetic ion on the B-site typically favors $J_2 > 0$ which agrees with the $\text{La}_2\text{MgIrO}_6$ result, while a d^{10} configuration of the B-site favors $J_2 < 0$, as for $\text{La}_2\text{ZnIrO}_6$. We note that the Heisenberg-Ising model description of the combined INS and thermodynamic data for $\text{La}_2\text{B}^{\text{II}}\text{IrO}_6$, which, as discussed above, requires $J_2 < 0$ for both the Mg and Zn materials, would not be consistent with this empirical correlation.

VII. VII. DISORDER EFFECTS

Our theoretical modeling above has considered the ideal fcc lattice or weak anisotropies induced by small non-cubic distortions. However, it is well known that B/B' site mixing may play an important role in DPs^{75,76}. The density of antisite

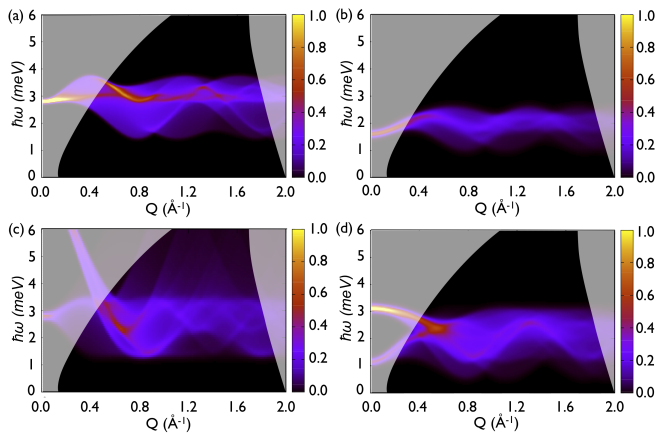


FIG. 5: (Color online) Illustrative plots of $S(Q, \omega)$ for the Heisenberg-Ising models and Kitaev-Heisenberg models. We have incorporated the Ir^{4+} form factor, and also used the instrumental energy resolution and the kinematic cutoff corresponding to the HYSPEC instrument with a neutron incident energy $E_i = 7.5$ meV. (a) Heisenberg-Ising model for $\text{La}_2\text{MgIrO}_6$ with $J_1 = 0.5$ meV, a second neighbor FM Heisenberg coupling $J_2 = -0.3J_1$, and uniaxial anisotropies $\lambda_1 = \lambda_2 = 1$. (b) Heisenberg-Ising model for $\text{La}_2\text{ZnIrO}_6$, with $J_1 = 0.2$ meV, $J_2 = -J_1$, and $\lambda_1 = \lambda_2 = 1$. (c) Kitaev-dominant model for $\text{La}_2\text{MgIrO}_6$ with $J_K = 1.7$ meV, anisotropy $\lambda_K = 0.2J_K$, and $J_2 = 0.2J_K$. (d) Kitaev-dominant model for $\text{La}_2\text{ZnIrO}_6$ with $J_K = 0.7$ meV, anisotropy $\lambda_K = 0.2J_K$, and second neighbor FM Heisenberg exchange $J_2 = -0.2J_K$.

defects n_d is commonly estimated from structural refinements of DP diffraction data, although it was previously assumed that this effect is negligible for $\text{La}_2\text{B}(\text{IrO}_6)$ in Ref.³³. We have therefore revisited the x-ray diffraction data presented in that paper and performed new structural refinements, with the site mixing included as a fitting parameter. We estimate a B/B' site mixing value of $\leq 8\%$ and $\leq 5\%$ for the Mg and Zn systems respectively, with lattice constants and atomic fractional coordinates essentially identical to the values reported in Ref.³³. Magnons scattering off such defects, with a magnon mean free path $\ell \sim n_d^{-1/3}$, will lead to momentum broadening $\Delta Q \sim 1/\ell$. Such disorder broadening may smear some of the sharp features in the theoretical $S(Q, \omega)$. Such disorder scattering, as well as the momentum broadening arising from finite instrument resolution, also not considered in the modeling, may further improve the agreement between theory and experiment.

VIII. VIII. CONCLUSIONS

In conclusion, we have carried out a joint experimental and theoretical investigation of the spin dynamics in the $j_{\text{eff}} = 1/2$ Mott insulators $\text{La}_2\text{B}(\text{IrO}_6)$. We have shown that we can explain the combined neutron and thermodynamic data with conventional Heisenberg-Ising models using significant ferromagnetic J_2 and a strong uniaxial Ising exchange interaction. The applicability of such models to the DP iridates is however not clear given their small monoclinic distortions. As an alter-

native, we have considered models with dominant Kitaev interactions - this unconventional form of exchange anisotropy is symmetry-allowed even on the ideal fcc lattice, and it leads to A-type AFM order, rather than an exotic quantum spin liquid. Indeed, we have shown that models with dominant Kitaev interactions, supplemented by weak anisotropies and small second neighbor couplings, appear to provide a natural alternative explanation of the INS data and thermodynamic measurements. Experiments probing spin dynamics in the small Q regime would be valuable in distinguishing these proposals.

Going beyond these specific materials, our work points to the possibility that such Kitaev-type directional exchange couplings induced by SOC may be the driving force responsible for the gapped A-type AFM states found in a variety of other $4d/5d$ -based DPs^{50,77-80}. This calls for *ab initio* studies of exchange interactions in such Mott insulating DP materials. In future work, it would be useful to synthesize single crystals of $\text{La}_2\text{B}(\text{IrO}_6)$ and other DPs. Studying the magnetic susceptibility and magnetic excitations from such single crystals might further serve to distinguish models with dominant Kitaev exchange from competing conventional models with dominant uniaxial Ising interactions. Finally, our work supports the idea that materials with multiple interfering Ir-O-O-Ir superexchange paths might be promising candidates for exploring Kitaev interactions on various lattice geometries.

Acknowledgments

We thank M.D. Lumsden, S.E. Nagler, and K.W. Plumb for useful discussions and V. O. Garlea for technical support. This research was supported by the US Department of Energy (DOE), Office of Basic Energy Sciences. Inelastic neutron scattering experiments were performed at the Spallation Neutron Source and the High Flux Isotope Reactor, which are sponsored by the Scientific User Facilities Division. A.A.A. and S.C. were supported by the Scientific User Facilities Division. G.-X.C. and D.M. were supported by the Materials Science and Engineering Division. T.J.W. acknowledges support from the Wigner Fellowship program at ORNL. A.M.C., Y.B.K., and A.P. were funded by NSERC of Canada.

Appendix A: Appendix: Mean field theory of gapped magnons

Beyond linear spin waves, we set for spin-1/2,

$$S_{\mathbf{r}}^x = (-1)^z \left(\frac{1}{2} - a_{\mathbf{r}}^\dagger a_{\mathbf{r}} \right) \quad (\text{A1})$$

$$S_{\mathbf{r}}^y = \frac{1}{2} (a_{\mathbf{r}} + a_{\mathbf{r}}^\dagger) - \frac{1}{4} (a_{\mathbf{r}}^\dagger a_{\mathbf{r}} a_{\mathbf{r}} + a_{\mathbf{r}}^\dagger a_{\mathbf{r}}^\dagger a_{\mathbf{r}}) \quad (\text{A2})$$

$$S_{\mathbf{r}}^z = (-1)^z \left[\frac{1}{2i} (a_{\mathbf{r}} - a_{\mathbf{r}}^\dagger) - \frac{1}{4i} (a_{\mathbf{r}}^\dagger a_{\mathbf{r}} a_{\mathbf{r}} - a_{\mathbf{r}}^\dagger a_{\mathbf{r}}^\dagger a_{\mathbf{r}}) \right] \quad (\text{A3})$$

and expand the Kitaev model Hamiltonian, only keeping terms to quartic order, which we decouple using mean field parameters $F_{\mathbf{k}} = \langle a_{\mathbf{k}}^\dagger a_{-\mathbf{k}}^\dagger \rangle$ and $G_{\mathbf{k}} = \langle a_{\mathbf{k}}^\dagger a_{\mathbf{k}} \rangle$. This leads to

the Hamiltonian:

$$H_{\text{mft}} = J_K \sum_{\mathbf{k}>0} \begin{pmatrix} a_{\mathbf{k}}^\dagger & a_{-\mathbf{k}} \end{pmatrix} \begin{pmatrix} A_{\mathbf{k}} & B_{\mathbf{k}} \\ B_{\mathbf{k}} & A_{\mathbf{k}} \end{pmatrix} \begin{pmatrix} a_{\mathbf{k}} \\ a_{-\mathbf{k}}^\dagger \end{pmatrix} \quad (\text{A4})$$

with $A_{\mathbf{k}} = (2 + C_{xy} + C_{xz}) + \delta A_{\mathbf{k}}$, $B_{\mathbf{k}} = (C_{xz} - C_{xy}) + \delta B_{\mathbf{k}}$, and

$$\begin{aligned} \delta A_{\mathbf{k}} &= 2(\bar{F}_{xy} - \bar{F}_{xz}) + \bar{F}(C_{xy} - C_{xz}) - 2\bar{G}(C_{xy} + C_{xz}) \\ &\quad - 2(\bar{G}_{xy} + \bar{G}_{xz}) - 4\bar{G} - 4\bar{G}_{yz}C_{yz} \quad (\text{A5}) \\ \delta B_{\mathbf{k}} &= (\bar{G}_{xy} - \bar{G}_{xz}) + 2\bar{G}(C_{xy} - C_{xz}) - \bar{F}(C_{xy} + C_{xz}) \\ &\quad - (\bar{F}_{xy} + \bar{F}_{xz}) - 4\bar{F}_{yz}C_{yz}. \quad (\text{A6}) \end{aligned}$$

Here, we have defined averages $\bar{F} \equiv \int_{\mathbf{k}} F_{\mathbf{k}}$, $\bar{F}_{ij} \equiv \int_{\mathbf{k}} C_{\mathbf{k}}^{ij} F_{\mathbf{k}}$, and similarly for $G_{\mathbf{k}}$. Requiring self-consistency, we set $\bar{F}_{\mathbf{k}} = \sinh 2\varphi_{\mathbf{k}}$ and $G_{\mathbf{k}} = (\cosh 2\varphi_{\mathbf{k}} - 1)/2$, with the renormalized dispersion $\Omega_{\mathbf{k}} = J_K \sqrt{A_{\mathbf{k}}^2 - B_{\mathbf{k}}^2}$, $\cosh 2\varphi_{\mathbf{k}} = A_{\mathbf{k}}/\Omega_{\mathbf{k}}$, and $\sinh 2\varphi_{\mathbf{k}} = -B_{\mathbf{k}}/\Omega_{\mathbf{k}}$. To solve these equations, we begin with a guess for the Hamiltonian matrix of the form $\delta A_{\mathbf{k}} = \gamma$, and $\delta B_{\mathbf{k}} = 0$, where γ represents the effect of the pinning field arising from order-by-disorder as described in

the text. We then iterate the mean field equations to achieve self-consistency.

We can use these converged results to also compute the resulting dynamic structure factor, which has components

$$\begin{aligned} \mathcal{S}_{xx}(\mathbf{q}, \omega) &= \frac{1}{4} \int \frac{d^3\mathbf{p}}{(2\pi)^3} (\sinh 2\varphi_{\mathbf{p}} \sinh 2\varphi_{\mathbf{q}+\mathbf{p}+\mathbf{G}} \\ &\quad + 4\cosh^2\varphi_{\mathbf{p}} \sinh^2\varphi_{\mathbf{q}+\mathbf{p}+\mathbf{G}}) \delta(\omega - \Omega_{\mathbf{p}} - \Omega_{\mathbf{q}+\mathbf{p}+\mathbf{G}}) \\ \mathcal{S}_{yy}(\mathbf{q}, \omega) &= (\cosh 2\varphi_{\mathbf{q}} + \sinh 2\varphi_{\mathbf{q}})(1 - 2\bar{G} - \bar{F}) \delta(\omega - \Omega_{\mathbf{q}}) \\ \mathcal{S}_{zz}(\mathbf{q}, \omega) &= (\cosh 2\varphi_{\mathbf{q}} - \sinh 2\varphi_{\mathbf{q}})(1 - 2\bar{G} + \bar{F}) \delta(\omega - \Omega_{\mathbf{q}+\mathbf{G}}) \end{aligned}$$

where $\mathbf{G} \equiv (0, 0, \pi)$. The first term corresponds to longitudinal fluctuations while the latter two correspond to transverse fluctuations. We find, numerically, that the longitudinal fluctuations make a very small contribution to the structure factor, and can be ignored in practice. Powder averaging leads to $S(Q, \omega)$, with $Q = |\vec{q}|$, which we convolute with a Gaussian function representing the instrumental energy resolution, and plot in Fig. 4(f) above.

- * author to whom correspondences should be addressed: E-mail:[aczela@ornl.gov]
- † author to whom correspondences should be addressed: E-mail:[arunp@physics.utoronto.ca]
- ¹ H. Yoshizawa, K. Hirakawa, S.K. Satija, and G. Shirane, Phys. Rev. B **23**, 2298 (1981).
 - ² S.E. Nagler, W.J.L. Buyers, R.L. Armstrong, and B. Briat, Phys. Rev. B **28**, 3873 (1983).
 - ³ A.W. Kinross, M. Fu, T.J. Munsie, H.A. Dabkowska, G.M. Luke, S. Sachdev, and T. Imai, Phys. Rev. X **4**, 031008 (2014).
 - ⁴ J.S. Gardner, M.J.P. Gingras, and J.E. Greedan, Rev. Mod. Phys. **82**, 53 (2010).
 - ⁵ C. Castelnuovo, R. Moessner, and S.L. Sondhi, Nature **451**, 42 (2008).
 - ⁶ K.A. Ross, L. Savary, B.D. Gaulin, and L. Balents, Phys. Rev. X **1**, 021002 (2011).
 - ⁷ B.J. Kim, H. Jin, S.J. Moon, J.-Y. Kim, B.-G. Park, C.S. Leem, J. Yu, T.W. Noh, C. Kim, S.-J. Oh, J.-H. Park, V. Durairaj, G. Cao, and E. Rotenberg, Phys. Rev. Lett. **101**, 076402 (2008).
 - ⁸ G. Jackeli and G. Khaliullin, Phys. Rev. Lett. **102**, 017205 (2009).
 - ⁹ J. Kim, D. Casa, M.H. Upton, T. Gog, Y.-J. Kim, J.F. Mitchell, M. van Veenendaal, M. Daghofer, J. van den Brink, G. Khaliullin, and B.J. Kim, Phys. Rev. Lett. **108**, 177003 (2012).
 - ¹⁰ J. Kim, A.H. Said, D. Casa, M.H. Upton, T. Gog, M. Daghofer, G. Jackeli, J. van den Brink, G. Khaliullin, and B.J. Kim, Phys. Rev. Lett. **109**, 157402 (2012).
 - ¹¹ A. Kitaev, Annals of Physics **321**, 2 (2006).
 - ¹² Y. Singh, S. Manni, J. Reuther, T. Berlijn, R. Thomale, W. Ku, S. Trebst, and P. Gegenwart, Phys. Rev. Lett. **108**, 127203 (2012).
 - ¹³ Y. Singh and P. Gegenwart, Phys. Rev. B **82**, 064412 (2010).
 - ¹⁴ K.W. Plumb, J.P. Clancy, L.J. Sandilands, V.V. Shankar, Y.F. Hu, K.S. Burch, H.-Y. Kee, and Y.-J. Kim, Phys. Rev. B **90**, 041112(R) (2014).
 - ¹⁵ F. Ye, S. Chi, H. Cao, B.C. Chakoumakos, J.A. Fernandez-Baca, R. Custelcean, T.F. Qi, O.B. Korneta, and G. Cao, Phys. Rev. B **85**, 180403(R) (2012).
 - ¹⁶ J.A. Sears, M. Songvilay, K.W. Plumb, J.P. Clancy, Y. Qiu, Y.

- Zhao, D. Parshall, and Y.-J. Kim, Phys. Rev. B **91**, 144420 (2015).
- ¹⁷ J. Chaloupka, G. Jackeli, and G. Khaliullin, Phys. Rev. Lett. **105**, 027204 (2010).
- ¹⁸ I. Kimchi and Y.-Z. You, Phys. Rev. B **84**, 180407 (2011).
- ¹⁹ J. G. Rau, E.K.-H. Lee, and H.-Y. Kee, Phys. Rev. Lett. **112**, 077204 (2014).
- ²⁰ Y. Sizyuk, C. Price, P. Wölfle, N. B. Perkins, Phys. Rev. B **90**, 155126 (2014).
- ²¹ J. Knolle, G.-W. Chern, D. L. Kovrizhin, R. Moessner, N. B. Perkins, Phys. Rev. Lett. **113**, 187201 (2014).
- ²² L.J. Sandilands, Y. Tian, K.W. Plumb, Y.-J. Kim, and K.S. Burch, Phys. Rev. Lett. **114**, 147201 (2015).
- ²³ J. Knolle, D. L. Kovrizhin, J. T. Chalker, and R. Moessner, Phys. Rev. Lett. **112**, 207203 (2014).
- ²⁴ A. Banerjee, C.A. Bridges, J.-Q. Yan, A.A. Aczel, L. Li, M.B. Stone, G.E. Granroth, M.D. Lumsden, Y. Yiu, J. Knolle, S. Bhatnagar, D.L. Kovrizhin, R. Moessner, D.A. Tennant, D.G. Mandrus, and S.E. Nagler, doi: 10.1038/nmat4604 (2016).
- ²⁵ T. Takayama, A. Kato, R. Dinnebier, J. Nuss, H. Kono, L.S.I. Veiga, G. Fabbris, D. Haskel, and H. Takagi, Phys. Rev. Lett. **114**, 077202 (2015).
- ²⁶ K.A. Modic, T.E. Smidt, I. Kimchi, N.P. Breznay, A. Biffin, S. Choi, R.D. Johnson, R. Coldea, P. Watkins-Curry, G.T. McCandless, J.Y. Chan, F. Gandara, Z. Islam, A. Vishwanath, A. Shekhter, R.D. McDonald, and J.G. Analytis, Nature Communications **5**, 4203 (2014).
- ²⁷ A. Biffin, R.D. Johnson, S. Choi, F. Freund, S. Manni, A. Bombardi, P. Manuel, P. Gegenwart, and R. Coldea, Phys. Rev. B **90**, 205116 (2014).
- ²⁸ A. Biffin, R.D. Johnson, I. Kimchi, R. Morris, A. Bombardi, J.G. Analytis, A. Vishwanath, and R. Coldea, Phys. Rev. Lett. **113**, 197201 (2014).
- ²⁹ E.K.-H. Lee and Y. B. Kim, Phys. Rev. B **91**, 064407 (2015).
- ³⁰ I. Kimchi, R. Coldea, and A. Vishwanath, Phys. Rev. B **91**, 245134 (2015).
- ³¹ I. Kimchi and A. Vishwanath, Phys. Rev. B **89**, 014414 (2014).
- ³² R.C. Currie, J.F. Vente, E. Frikkee, and D.J.W. Ijdo, Journal of

- Solid State Chemistry **116**, 199 (1995).
- ³³ G.-X. Cao, A. Subedi, S. Calder, J.-Q. Yan, J. Yi, Z. Gai, L. Poudel, D.J. Singh, M.D. Lumsden, A.D. Christianson, B.C. Sales, and D. Mandrus, *Phys. Rev. B* **87**, 155136 (2013).
- ³⁴ W.K. Zhu, C.-K. Lu, W. Tong, J.M. Wang, H.D. Zhou, and S.X. Zhang, *Phys. Rev. B* **91**, 144408 (2015).
- ³⁵ M. Becker, M. Hermanns, B. Bauer, M. Garst, and S. Trebst, *Phys. Rev. B* **91**, 155135 (2015).
- ³⁶ A. Catuneanu, J. G. Rau, H.-S. Kim, and H.-Y. Kee, *Phys. Rev. B* **92**, 165108 (2015).
- ³⁷ G. Jackeli and A. Avella, *Phys. Rev. B* **92**, 184416 (2015).
- ³⁸ Ref.³⁴ suggests that there are actually two different magnetic transition temperatures in close proximity for $\text{La}_2\text{ZnIrO}_6$ ($T_1 = 7.3$ K and $T_2 = 8.5$ K), but this finding is not important for the results presented in our work.
- ³⁹ M.S. Seehra and T.M. Giebultowicz, *Phys. Rev. B* **38**, 11898 (1988).
- ⁴⁰ K. Lefmann and C. Rischel, *Eur. Phys. J. B* **21**, 313 (2001).
- ⁴¹ A.M. Cook, S. Matern, C. Hickey, A.A. Aczel, and A. Paramakanti, *Phys. Rev. B* **92**, 020417(R) (2015).
- ⁴² H. Gretarsson, J.P. Clancy, Y. Singh, P. Gegenwart, J.P. Hill, J. Kim, M.H. Upton, A.H. Said, D. Casa, T. Gog, and Y.-J. Kim, *Phys. Rev. B* **87**, 220407(R) (2013).
- ⁴³ W.A. Groen, F.P.F. van Berkel, and D.J.W. Ijdo, *Acta Cryst. C* **42**, 1472 (1986).
- ⁴⁴ A.M. Glazer, *Acta Cryst. B* **28**, 3384 (1972).
- ⁴⁵ P.M. Woodward, *Acta Cryst. B* **53**, 32 (1997).
- ⁴⁶ X. Liu, V.M. Katukuri, L. Hozoi, W.-G. Yin, M.P.M. Dean, M.H. Upton, J. Kim, D. Casa, A. Said, T. Gog, T.F. Qi, G. Cao, A.M. Tsvetlik, J. van den Brink, and J.P. Hill, *Phys. Rev. Lett.* **109**, 157401 (2012).
- ⁴⁷ H. Gretarsson, J.P. Clancy, X. Liu, J.P. Hill, E. Bozin, Y. Singh, S. Manni, P. Gegenwart, J. Kim, A.H. Said, D. Casa, T. Gog, M.H. Upton, H.-S. Kim, J. Yu, V.M. Katukuri, L. Hozoi, J. van den Brink, and Y.-J. Kim, *Phys. Rev. Lett.* **110**, 076402 (2013).
- ⁴⁸ T. Dodds, T.-P. Choy, and Y.-B. Kim, *Phys. Rev. B* **84**, 104439 (2011).
- ⁴⁹ H. Ishizuka and L. Balents, *Phys. Rev. B* **90**, 184422 (2014).
- ⁵⁰ A.E. Taylor, R. Morrow, R.S. Fishman, S. Calder, A.I. Kolesnikov, M.D. Lumsden, P.M. Woodward, and A.D. Christianson, arXiv: 1511.07486 (unpublished).
- ⁵¹ S.E. Nagler, W.J.L. Buyers, R.L. Armstrong, and B. Briat, *Phys. Rev. B* **27**, 1784 (1983).
- ⁵² U. Tellenbach, *J. Phys. C: Solid State Phys.* **11**, 2287 (1978).
- ⁵³ T. Nguyen, S.E. Nagler, R.A. Cowley, T. Perring, and R. Osborn, *J. Phys.: Condens. Matter* **7**, 2917 (1995).
- ⁵⁴ E.V. Kuz'min, S.G. Ovchinnikov, and D.J. Singh, *Phys. Rev. B* **68**, 024409 (2003).
- ⁵⁵ S. Boseggia, H. C. Walker, J. Vale, R. Springell, Z. Feng, M. Moretti Sala, H. M. Ronnow, S.P. Collins, D.F. McMorrow, *J. Phys.: Cond. Matt.* **25**, 422202 (2013).
- ⁵⁶ F. Wang and T. Senthil, *Phys. Rev. Lett.* **106**, 136402 (2011).
- ⁵⁷ S. Fujiyama, H. Ohsumi, T. Komesu, J. Matsuno, B.J. Kim, M. Takata, T. Arima, and H. Takagi, *Phys. Rev. Lett.* **108**, 247212 (2012).
- ⁵⁸ S. Bahr, A. Alfonsov, G. Jackeli, G. Khaliullin, A. Matsumoto, T. Takayama, H. Takagi, B. Buchner, and V. Kataev, *Phys. Rev. B* **89**, 180401(R) (2014).
- ⁵⁹ S. Boseggia, R. Springell, H.C. Walker, A.T. Boothroyd, D. Prabhakaran, D. Wermeille, L. Bouchenoire, S.P. Collins, and D.F. McMorrow, *Phys. Rev. B* **85**, 184432 (2012).
- ⁶⁰ B. Halg and A. Furrer, *Phys. Rev. B* **34**, 6258 (1986).
- ⁶¹ While a small $J_1 > 0$ appears to be ultimately necessary for globally favoring the AFM-II state in the classical Heisenberg-Kitaev model, it does not qualitatively or quantitatively affect the spin-wave energetics around the A-II state for $J_1 \ll J_K$.
- ⁶² G. Khaliullin, *Phys. Rev. B* **64**, 212405 (2001).
- ⁶³ L. Savary, K. A. Ross, B. D. Gaulin, J.P.C. Ruff, and L. Balents, *Phys. Rev. Lett.* **109**, 167201 (2012).
- ⁶⁴ K. A. Ross, Y. Qiu, J. R. D. Copley, H. A. Dabkowska, B. D. Gaulin, *Phys. Rev. Lett.* **112**, 057201 (2014).
- ⁶⁵ J.-W. Bos and J.P. Attfield, *PRB* **70**, 174434 (2004).
- ⁶⁶ K.L. Holman, Q. Huang, T. Klimczuk, K. Trzebiatowski, J.W.G. Bos, E. Morosan, J.W. Lynn, and R.J. Cava, *Journal of Solid State Chemistry* **180**, 75 (2007).
- ⁶⁷ D.E. Cox, G. Shirane, and B.C. Frazer, *Journal of Applied Physics* **38**, 1459 (1967).
- ⁶⁸ S. Vasala, M. Avdeev, S. Danilkin, O. Chmaissem, and M. Karppinen, *J. Phys.: Condens. Matter* **26**, 496001 (2014).
- ⁶⁹ T. Koga, N. Kurita, M. Avdeev, S. Danilkin, T.J. Sato, and H. Tanaka, *PRB* **93**, 054426 (2016).
- ⁷⁰ M. Retuerto, M. Garcia-Hernandez, M.J. Martinez-Lope, M.T. Fernandez-Diaz, J.P. Attfield, and J.A. Alonso, *J. Mater. Chem.* **17**, 3555 (2007).
- ⁷¹ K. Chakraborty, A. Das, P.S.R. Krishna, S.M. Yusuf, S.J. Patwe, S.N. Achary, and A.K. Tyagi, *Journal of Alloys and Compounds* **457**, 15 (2008).
- ⁷² T. Kumar Mandal, A.M. Abakumov, M.V. Lobanov, M. Croft, V.V. Poltavets, and M. Greenblatt, *Chem. Mater.* **20**, 4653 (2008).
- ⁷³ M.C. Viola, M.J. Martinez-Lope, J.A. Alonso, J.L. Martinez, J.M. De Paoli, S. Pagola, J.C. Pedregosa, M.T. Fernandez-Diaz, and R.E. Carbonio, *Chem. Mater.* **15**, 1655 (2003).
- ⁷⁴ L. Ortega-San Martin, J.P. Chapman, L. Lezama, J. Sanchez Marcos, J. Rodriguez-Fernandez, M.I. Arriortua, and T. Rojo, *Eur. J. Inorg. Chem.* **2006**, 1362 (2006).
- ⁷⁵ Q.S. Lin, M. Greenblatt, E.N. Caspi, and M. Avdeev, *Journal of Solid State Chemistry* **179**, 2086 (2006).
- ⁷⁶ T. Aharen, J.E. Greedan, C.A. Bridges, A.A. Aczel, J. Rodriguez, G. MacDougall, G.M. Luke, T. Imai, V.K. Michaelis, S. Kroeker, H. Zhou, C.R. Wiebe, and L.M.D. Cranswick, *Phys. Rev. B* **81**, 224409 (2010).
- ⁷⁷ E. Kermarrec, C.A. Marjerrison, C.M. Thompson, D.D. Maharaj, K. Levin, S. Kroeker, G.E. Granroth, R. Flacau, Z. Yamani, J.E. Greedan, and B.D. Gaulin, *Phys. Rev. B* **91**, 075133 (2015).
- ⁷⁸ A.E. Taylor, R. Morrow, D.J. Singh, S. Calder, M.D. Lumsden, P.M. Woodward, and A.D. Christianson, *Phys. Rev. B* **91**, 100406(R) (2015).
- ⁷⁹ P.D. Battle and C.W. Jones, *Journal of Solid State Chemistry* **78**, 108 (1989).
- ⁸⁰ J.P. Carlo, J.P. Clancy, K. Fritsch, C.A. Marjerrison, G.E. Granroth, J.E. Greedan, H.A. Dabkowska, and B.D. Gaulin, *Phys. Rev. B* **88**, 024418 (2013).